Journal of Materials Chemistry A

Accepted Manuscript

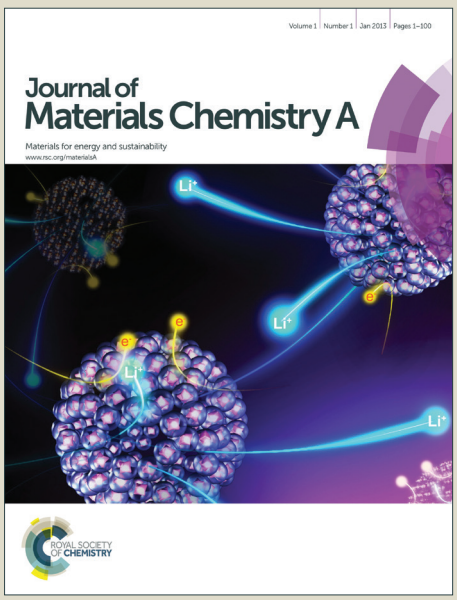

ROYAL SOCIETY OF CHEMISTRY

www.rsc.org/materialsA

Journal of Materials Chemistry A RSCPublishing

ARTICLE

A Direct One-Step Synthetic Route to Pd-Pt Nanostructures with Controllable Shape, Size, and Composition for Electrocatalytic Applications

Youngjin Ye,[a] Jin Joo,[b] Seongggyu Lee[a] and Jinwoo Lee[a, *]

Cite this: DOI: 10.1039/x0xx00000x

Received 00th January 2012,
Accepted 00th January 2012

DOI: 10.1039/x0xx00000x

www.rsc.org/

Pd-Pt branched nanocrystals have been known to exhibit a synergistic effect in many electrocatalytic reactions such as reduction of oxygen and oxidation of small organic molecules. However, Pd-Pt branched structures have generally been synthesized using a two-step seed-mediated approach, which is unbeneficial for large-scale synthesis. Therefore, it is necessary to develop a one-step route to Pd-Pt branched structures. Herein, we developed a direct one-step synthetic route to obtain Pd-Pt structures with controllable shape, size, and composition. In this system, KBr plays a critical role in controlling the size and shape of the Pd-Pt NCs. The resulting Pd_1Pt_5 branched nanocrystals showed 3.4 and 6.2 times higher mass activity toward oxygen reaction and formic acid oxidation than commercial Pt/C, respectively.

Introduction

Platinum (Pt) nanocrystals (NCs) have attracted significant interest because of their wide range of applications, particularly in catalysis.[1-4] Recent studies have revealed that the morphology of nanoparticles directly affects their chemical reactivity by determining the bounding facets of the nanoparticles, as well as the number of step edges and kink sites.[1-3, 5-7] Therefore, the rational design and synthesis of Pt NCs offers great advantages for the precise control of the active sites to maximize the catalytic activity of NCs. In predicting and controlling the shape of Pt NCs, it is crucial to consider the surface energy. Pt NCs, which have a face-centered cubic (fcc) lattice, are usually bound by low-index {111}, {100}, and {110} planes. Because the surface energy increases in the order $\gamma\{111\} < \gamma\{100\} < \gamma\{110\}$, a truncated octahedron bound by the {111} and {100} facets has the minimum surface energy and is the most favorable.[8] Therefore, Pt NCs have no intrinsic driving force for anisotropic growth, making the shape control of Pt NCs challenging.[9]

Current advances in nanotechnology have allowed us to tune the size and shape of NCs.[2, 10, 11] A variety of Pt nanostructures, including one-dimensional,[12-15] cubic,[16-19] polyhedral,[20-24] and branched[9, 25-32] structures have been realized so far. Among the various structures mentioned above, branched structures have attracted great interest owing to their high surface area, well-defined facets, and rough surfaces.[9, 26-31] The exposure of high-index facets, steps, and kinks from the rough surfaces of branched structures provides high catalytic activity not afforded by spherical NCs with smooth surfaces. In addition to the shape of NCs, the catalytic activity is also highly dependent on the composition of the NCs.[2, 4, 33, 34] A wide range of bi- or tri-metallic Pt-based NCs, including Pd-Pt,[35-41] Au-Pt,[42, 43] and Au-Pd-Pt,[38, 44] have been extensively explored. Among them, Pd-Pt bimetallic NCs have been known to exhibit a synergistic effect in many reactions, such as the reduction of oxygen[35, 40] and the oxidation of small organic molecules.[36, 38] Pd-Pt bimetallic NCs provide additional advantages in controlling the shape of NCs because both Pd and Pt have an fcc lattice with a very small lattice mismatch of 0.77%, making overgrowth favorable.[37] Pd-Pt branched structures have been extensively studied and observed to exhibit exciting electrocatalytic activity.[35-39, 41]

Generally, Pd-Pt branched structures have been synthesized using a two-step seed-mediated approach.[35-37] Well-faceted Pd seeds provide multiple attachment sites for Pt nanoparticles. This is helpful in avoiding overlap and fusion between Pt branches during their growth.[35, 36] Without the use of pre-synthesized Pd seeds, the size and shape of Pd-Pt NCs were uncontrollable, thus resulting in dense and foam-like Pt aggregates rather than open porous dendrites.[36] From a practical point of view, a direct one-step route to bimetallic NCs would be ideal for large-scale synthesis. Since the catalytic activity of NCs is highly dependent on size, shape, and composition,[2, 3] rapid synthetic route with predictable control over morphology and composition would open up the possibilities of screening efficient catalysts in various kinds of catalysis. Recently, direct one-step syntheses of Pd-Pt,[38, 39], Au-Pt,[45] Au-Pd-Pt,[44] and Ni-Pt[46, 47] branched structures have been reported. However, there

is still a lack of direct synthetic routes with systematic control over the shape, size, and composition of branched Pt-based bimetallic structures.

Herein, we developed a direct one-step synthetic route to obtain Pd-Pt structures with controllable shape, size, and composition. The Pd-Pt NCs were prepared using chloroplatinic acid hexahydrate ($H_2PtCl_6 \cdot 6H_2O$) and sodium tetrachloropalladate (Na_2PdCl_4) as precursors, L-ascorbic acid as a reducing agent, polyvinylpyrrolidone (PVP) as a surfactant, and KBr as a structure-directing agent. In a typical synthesis of branched Pd-Pt NCs, $H_2PtCl_6 \cdot 6H_2O$, Na_2PdCl_4, L-ascorbic acid, PVP, and KBr were thoroughly mixed in DI water. The homogeneous mixture was then heated at 80 ºC for 3 h, yielding Pd-Pt NCs. In this system, KBr plays a critical role in controlling the size and shape of the Pd-Pt NCs. By varying the amount of KBr, we were able to synthesize Pd_1Pt_5 branched structures with particle sizes of 15, 17, 25, 30, and 38 nm. Moreover, various nanostructures with different compositions were successfully synthesized using this method (Fig. 1).

High-resolution TEM (HRTEM) analysis showed that the Pd_1Pt_5 NCs have porous structures with spatially separated and well-faceted branches. Thus, they are expected to possess high electrocatalytic activity. As a model system to show the shape-dependent catalytic activity, Pd_1Pt_5 branched structures were tested as electrocatalysts for the oxygen reduction reaction (ORR) and formic acid oxidation reaction (FAOR). Pd_1Pt_5 branched NCs showed greatly enhanced catalytic activity (0.314 $mA \cdot cm^{-2}_{Pt}$, 0.192 $mA \cdot \mu g^{-1}_{Pt}$) compared to commercial Pt/C (Johnson-Matthey, 20 wt% Pt, 0.088 $mA \cdot cm^{-2}_{Pt}$, 0.056 $mA \cdot \mu g^{-1}_{Pt}$) for the ORR at 0.9 V. They also showed greatly enhanced catalytic activity (0.452 $mA \cdot \mu g^{-1}_{Pt}$) over Pt/C (0.073 $mA \cdot \mu g^{-1}_{Pt}$) for the FAOR at 0.5 V.

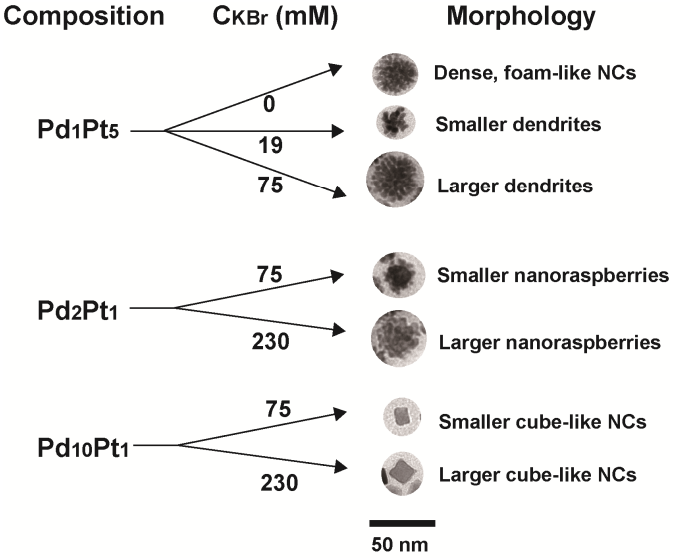

Fig. 1. Schematic figure showing the various Pd-Pt NCs synthesized by controlling the composition and the concentration of KBr.

Experimental Section

Synthesis of Pd-Pt NCs

Before synthesis, aqueous solutions of Na_2PdCl_4 (57 $mg \cdot mL^{-1}$) and $H_2PtCl_6 \cdot 6H_2O$ (57 $mg \cdot mL^{-1}$) were prepared and stored away from light. For the preparation of Pd-Pt NCs, 105 mg of PVP (MW=55,000), 60 mg of L-ascorbic acid, and the desired amount of KBr were dissolved in 10 mL of water. The desired amount of Na_2PdCl_4 solution and $H_2PtCl_6 \cdot 6H_2O$ solution were injected into the vial. Total solution volume was controlled to 11 mL. For example, for the preparation of Pd_1Pt_5 NCs, 0.1 mL of Na_2PdCl_4 solution and 0.9 mL of $H_2PtCl_6 \cdot 6H_2O$ solution were injected into the vial. The reaction vial was then placed into an oil bath preheated to 80 ºC. After a 3 h reaction time, the vial was cooled to RT. The synthesized nanoparticles were isolated by centrifugation with water and acetone two times. The product was further washed by centrifugation with 200 µL of a 30% H_2O_2 solution, 0.5 mL of concentrated H_2SO_4, and 8 mL of DI water. [48] The resulting product was then centrifuged with ethanol and hexane to remove the remaining H_2O_2 and H_2SO_4 in the solution. The Pd-Pt NCs were redispersed in ethanol for further characterization.

Physical Characterization

Transmission electron microscope (TEM) images of the Pd-Pt NCs were obtained using a JEM-2010 (JEOL) and JEM-2200FS (JEOL). Electron energy loss spectroscopy (EELS) mapping images were obtained using a JEM-2200FS (JEOL). Powder X-ray diffraction (XRD) patterns were obtained using a Bruker D8 Advanced X-ray diffractometer with Cu Kα radiation (λ = 0.15418 nm). The amount of metal in the PdPt/C was determined with an inductively coupled plasma-atomic emission spectrometer (ICP-AES) (ICPE-9000, Shimadzu).

Electrochemical Characterization

The electrochemical characterization was performed in a three-electrode cell with a rotating disk electrode (Pine Research Instrumentation) connected to a potentiostat (Gamry Reference 600, Gamry Instruments). Ag/AgCl (3 M NaCl) and Pt wire were used as reference and counter electrodes, respectively. 0.1 M $HClO_4$ electrolyte was prepared by diluting 70 % $HClO_4$ (Sigma-Aldrich) with DI water. The catalyst dispersions were prepared by dispersing the catalysts in a solution containing water, isopropanol, and 5 wt% Nafion® solution (V_{water}:$V_{2\text{-}propanol}$:$V_{5\ wt\%\ Nafion\ solution}$ = 1:4:0.05), followed by sonication for 30 min. The loading of Pt on glassy carbon was controlled at ~16 $\mu g \cdot cm^{-2}_{disk}$.

After the electrolyte was saturated with Ar, CV was recorded with a sweep rate of 50 $mV \cdot s^{-1}$ at room temperature (RT) until a stable CV was obtained. The electrochemical surface areas of the catalysts were determined from the hydrogen desorption region ($0.05 < E < 0.4$ V versus reversible hydrogen electrode (RHE)), assuming 210 $\mu C \cdot cm^{-2}_{Pt}$ for a monolayer adsorption of hydrogen on a Pt surface. After the electrolyte was saturated with oxygen, oxygen reduction activities were measured in 0.1 M $HClO_4$ solutions at a sweep rate of 20 $mV \cdot s^{-1}$ and a rotation speed of 1600 rpm at RT. The kinetic current was obtained based on the Koutecky-Levich equation, which can be described as follows:

$$1/i = 1/i_d + 1/i_k = 1/(B\omega^{1/2}) + 1/i_k$$

where i is the measured current, i_d is the diffusion-limited current, i_k is the kinetic current, B is the constant, and ω is the rotation rate. Formic acid oxidation activities were measured in Ar-purged 0.25 M formic acid in 0.1 M $HClO_4$ solution at RT, with a sweep rate of 50 mV/s.

CO stripping experiments were carried out in 0.1 M $HClO_4$ solution. All procedures involving CO stripping should be carried out in a well-ventilated hood. After 0.1 M $HClO_4$ solution was purged by Ar for 30 min, CO was purged into the solution for 30 min while maintaining the potential at 0.07 V. After removing the dissolved CO gas by bubbling Ar gas for 30 min at an electrode potential at 0.07 V, CO stripping was obtained between 0.07 V and 0.95 V.

Results and Discussion

Figs. 2a and b show representative TEM images of the dendritic Pd_1Pt_5 NCs. Open porous dendrites, with an average size of 17.4 nm, rather than dense aggregates were formed in high yield (>90%). The HRTEM image of the Pd_1Pt_5 dendrites shown in Fig. 2c shows that the Pd_1Pt_5 dendrites have porous structures with spatially separated and well-faceted branches.

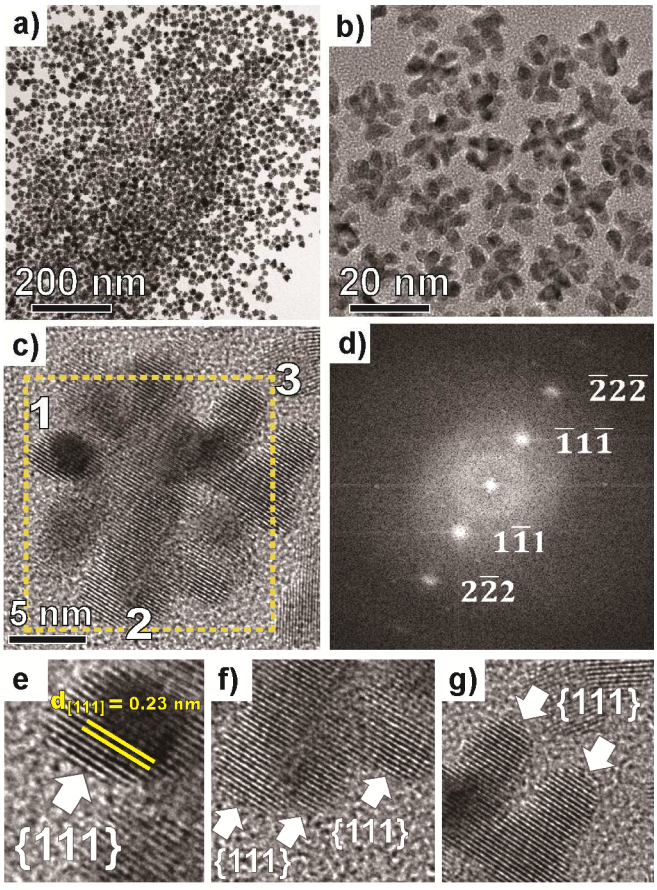

Fig. 2. (a) and (b) TEM images of the Pd_1Pt_5 dendrites. (c) HRTEM image and (d) corresponding FFT pattern of the Pd_1Pt_5 dendrites. (e-g) Magnified images of the branches of the Pd_1Pt_5 dendrites of the selected region marked in Fig. 2c.

The fast Fourier transform (FFT) pattern viewed along the [1 4 3] direction indicates that the dendritic Pd_1Pt_5 NC is almost single crystalline (Fig. 2d). Most of the exposed surfaces of the dendritic Pd_1Pt_5 NC were {111} facets (Figs. 2e–g). Further analysis of the exposed facets of the Pd_1Pt_5 dendrites using HRTEM and the corresponding FFT patterns confirms the preferential exposure of the {111} facets with some {100} and {110} facets (Fig. S1). The chemical structure of the Pd_1Pt_5 dendrites was analyzed using electron energy loss spectroscopy (EELS) mapping, which showed that the density of Pd atoms is higher in core part and the density of Pt atoms is higher in shell part of the Pd_1Pt_5 dendrites (Fig. S2).

The use of Pd is necessary to form an open porous structure. Without Pd, spherical NCs and dendritic NCs were formed separately, with a high relative standard deviation (RSD) of 36% (Fig. S3a). According to B. Lim *et al.*, during the growth of Pd-Pt dendrites using pre-formed Pd seeds, both homogeneous and heterogeneous nucleation of Pt occurred, and Pt branches were formed through the oriented attachment of small Pt NCs.[36] As shown in the TEM image of the Pd_1Pt_5 dendrites obtained after 10 min reaction time, both smaller spherical NCs and larger NCs with rough surfaces were found, supporting that the Pd-Pt NCs were formed by both homogeneous and heterogeneous nucleation (Fig. S4a). The heterogeneous nucleation is thermodynamically governed by the interplay between the strain energy, interfacial energy, and surface energy of the substrate and the deposit.[2, 36] Because Pd and Pt have a very small lattice mismatch of 0.77%, the growth of Pt on Pd occurs by the Volmer-Weber island growth mode, producing Pd-Pt dendrites (Fig. S4b). In the direct synthetic routes, the Pd and Pt precursors are reduced by L-ascorbic acid in the absence of pre-formed Pd seeds. Although the standard reduction potential of $[PtCl_6]^{2-}$/Pt (0.717 V vs. SHE) is higher than $[PdCl_4]^{2-}$/Pd (0.591 V vs. SHE), Pd NCs are formed before Pt to act as in situ seeds for the growth of Pt by providing attachment sites in this system.[38] Similar phenomena have been reported for synthesis of Pd-Pt[38, 49] and Au-Pd-Pt NCs.[44]

KBr played a critical role in the formation of the dendrites. Without KBr, foam-like Pd-Pt NCs with dense branches were formed with a high RSD of 31% (Fig. S3b). By varying the concentration of KBr, the size of the Pd_1Pt_5 dendrites can be tuned from 15 to 40 nm (Fig. 3a). As the concentration of KBr was increased, the size of the Pd_1Pt_5 dendrites increased, and the branches became denser (Figs. 3b–e). The average sizes and size distributions of the Pd_1Pt_5 dendrites are shown in Fig. S5 and Table S1. Br^- ions affect the shape of the in situ Pd seeds, changing the final morphology of the Pd_1Pt_5 dendrites. In addition, Br^- ions react with $[PdCl_4]^{2-}$ to produce $[PdBr_4]^{2-}$, slowing the reduction rate of the Pd precursor because the stability constant of $[PdBr_4]^{2-}$ is much higher than that of $[PdCl_4]^{2-}$.[50] Similarly, Br^- ions also affect the self-aggregation of Pt NCs by making effect on the reduction rate of Pt (Fig. S6).[29]

To further test the effect of the reduction rate on the morphology of the Pd-Pt NCs, KCl and KBr were added in

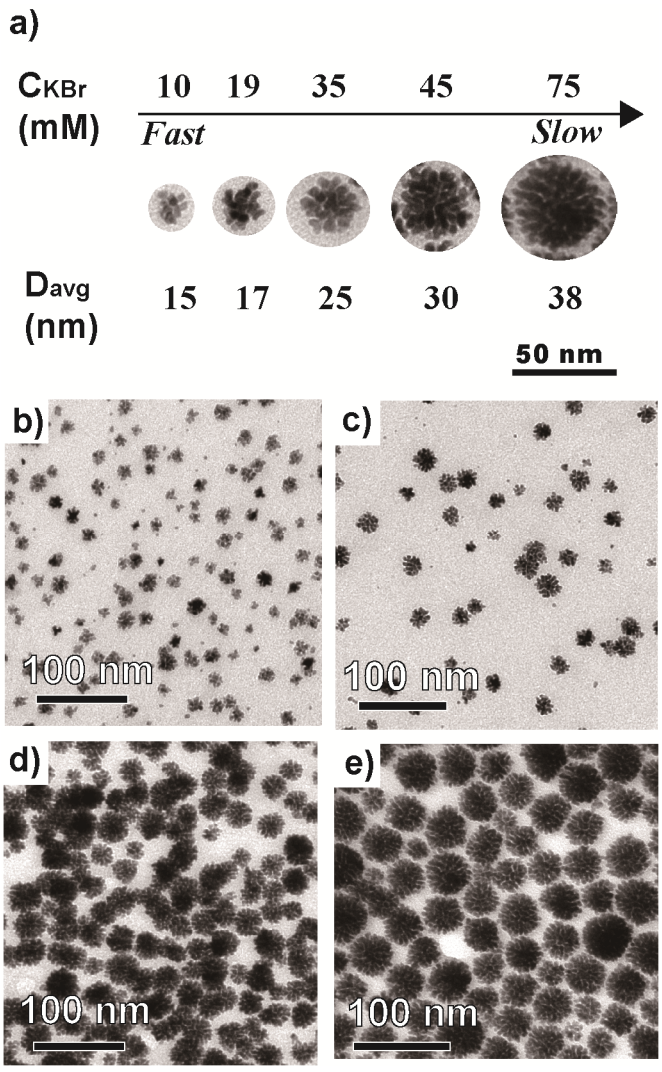

Fig. 3. (a) Schematic illustration showing the size increase of the Pd_1Pt_5 NCs with increasing KBr concentration. (b-e) TEM images of the Pd_1Pt_5 NCs prepared under the same conditions as in Fig. 2a, except the concentration of KBr was varied to be (b) 10, (c) 35, (d) 45, (e) 75 mM.

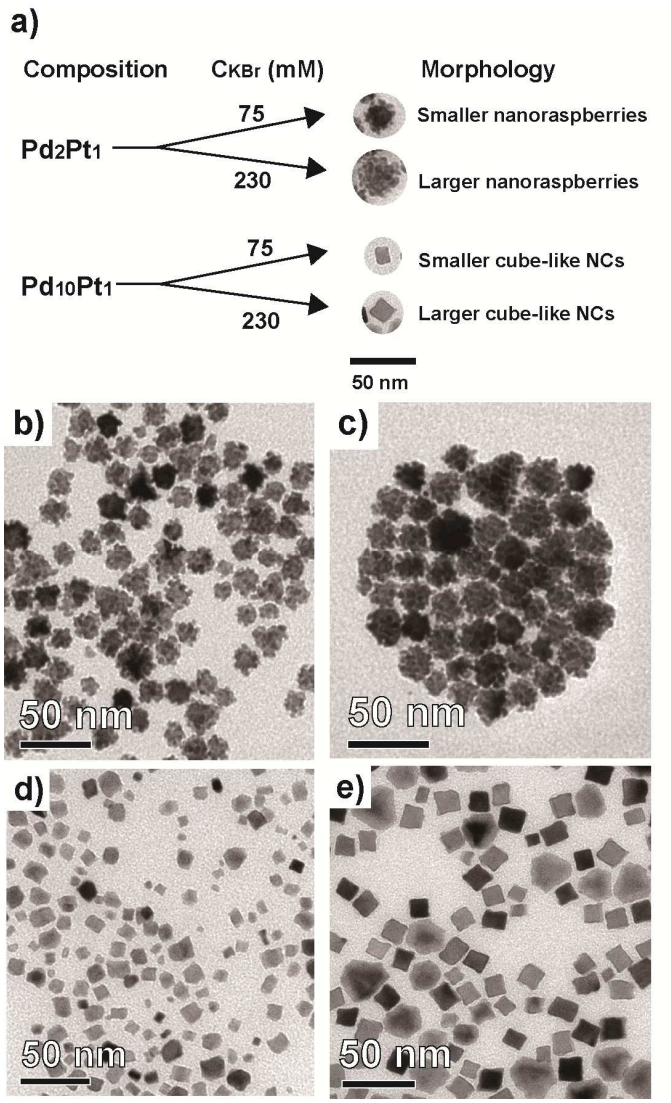

Fig. 4. (a) Schematic image for the synthesis of Pd_2Pt_1 nanoraspberries anc $Pd_{10}Pt_1$ cube-like NCs. (b-c) TEM images of the Pd_2Pt_1 NCs with KBr concentrations of (b) 75 and (c) 230 mM. (d-e) TEM images of the $Pd_{10}Pt_1$ NCs with KBr concentrations of (d) 75 and (e) 230 mM.

different molar ratios. Varying the molar ratio of different halide species is known to be an effective method to control the reduction rate of Pd precursors, because halide species such as Br^- and Cl^- have different binding strengths of Pd ions.[50] When the reduction rate of the precursors is relatively fast, *i.e.*, at a higher KCl/KBr molar ratio, dendritic NCs and individual spherical NCs were separately formed (Figs. S7a–b). As the molar ratio of KCl/KBr decreases and the reduction rate of the precursors becomes slower, the proportion of separate spherical NCs significantly decreases, whereas the proportion of dendritic NCs increases to nearly 100% (Figs. S7c–d). This result supports the conclusion that the slower reduction rates of the Pd and Pt precursors induced by Br^- ions affect the morphology of the Pd-Pt dendrites.

Pd-Pt NCs of various shapes were prepared by varying the concentration of Na_2PdCl_4, $H_2PtCl_6{\cdot}6H_2O$, and KBr (Fig. 4a). Figs. 4b and c shows the TEM images of the Pd_2Pt_1 NCs at KBr concentrations of 75 and 230 mM. Because KBr lowers the reduction rate of the precursors, the size of the Pd_2Pt_1 NCs increased, with denser branches, when the concentration of KBr was increased from 75 to 230 mM (Fig. S8 and Table S2). In case of Pd_2Pt_1 NCs, Pt grew on the in situ Pd by the Volmer-Weber growth mode, producing Pd-Pt nanoraspberries (Figs. 4b and c). TEM images of Pd_2Pt_1 NCs obtained after 25 min and 45 min reveal that both homogeneous and heterogeneous nucleation occurred, followed by the oriented attachment of Pd_2Pt_1 NCs (Fig. S9). In addition, the Pd_2Pt_1 nanoraspberries are composed of short and spherical branches rather than anisotropic and well-faceted branches. Anisotropic branches are formed when the rate of monomer addition to the seed is faster than the diffusion of the monomer.[26] In the formation of the Pd_1Pt_5 dendrites, owing to the slower reduction rate induced by Br^-, the concentration of the in situ Pd seeds was kept low, whereas that of the monomer was kept high. Therefore, the rate of monomer addition is faster than the rate of diffusion,

resulting in Pd-Pt NCs with anisotropic branches. As the concentration of Pd seeds increased and that of the monomer decreased, branches of Pd-Pt NCs become shorter and spherical (Fig. S10). Thus, Pd_2Pt_1 nanoraspberries composed of spherical branches were formed rather than anisotropic branches.

Figs. 4d and e shows the TEM images of the $Pd_{10}Pt_1$ NCs at KBr concentrations of 75 and 230 mM. The effect of KBr on Pd is increased, and therefore cube-like structures are formed. The average size of the $Pd_{10}Pt_1$ NCs increased with increasing concentrations of KBr (Fig. S8 and Table S2). In case of the $Pd_{10}Pt_1$ NCs, even at a relatively high KBr concentration of 230 mM, branched structures were not generated. In the formation of the $Pd_{10}Pt_1$ NCs, the concentration of the in situ Pd seeds is high, whereas that of Pt is low. Therefore, the available nucleation sites at the corners and edges of the in situ Pd seeds are sufficiently abundant to facilitate heterogeneous nucleation. As different from Pd_1Pt_5 and Pd_2Pt_1 NCs, smaller spherical NCs which might be formed by homogeneous nucleation were rarely found in TEM images of $Pd_{10}Pt_1$ NCs, further supporting the dominance of heterogeneous nucleation (Fig. S11). In addition, the rate of monomer addition becomes lower compared to the formation of the Pd_1Pt_5 and Pd_2Pt_1 NCs. The formation of the $Pd_{10}Pt_1$ NCs with smooth surfaces could be attributed to the relatively high degree of heterogeneous nucleation combined with the decreased rate of monomer addition.

Because the catalytic activity for the ORR and FAOR is highly structure-dependent, these reactions were selected as model systems to test for changes in the catalytic activity of shape-controlled Pd-Pt NCs. The Pd_1Pt_5 dendrites in Fig. 2a have an open porous structure, with anisotropic branches. Thus, they are expected to exhibit high electrocatalytic activity toward the ORR and FAOR. For electrochemical measurements, the Pd_1Pt_5 dendrites were thoroughly washed to remove excess PVP and then deposited on Vulcan XC-72 carbon. Fig. S12 shows the XRD pattern of the Pd_1Pt_5 NCs supported on carbon. The average crystallite size obtained using the Scherrer equation was 15.67 nm, which was similar to the average size calculated from the TEM image. In addition, (111)/(100) peak ratio of Pd_1Pt_5 NCs was 1.4 times higher than that of the bulk Pt structure, supporting the preferential exposure of {111} facets.[51]

Fig. 5a shows the cyclic voltammograms for the Pd_1Pt_5 dendrites recorded in Ar-purged 0.1 M $HClO_4$ solution. The electrochemical surface area (ECSA) of the Pd_1Pt_5 dendrites was determined from the H_{upd} adsorption between 0 and 0.4 V. The ECSA of the Pd_1Pt_5 dendrites was determined to be 61.06 $m^2 \cdot g^{-1}_{metal}$, which was slightly smaller than that of Pt/C (63.98 $m^2 \cdot g^{-1}_{Pt}$). The ORR activity of the Pd_1Pt_5 dendrites was characterized by polarization curves using rotating disk electrode (RDE) recorded at 1600 rpm (Fig. 5b). The half wave potential was 880 mV, which was 60 mV higher than that of Pt/C. At 0.9 V versus a reversible hydrogen electrode (RHE), the mass and specific activities of the Pd_1Pt_5 dendrites were determined to be 0.192 $mA \cdot \mu g^{-1}_{metal}$ and 0.314 $mA \cdot cm^{-2}_{metal}$, respectively. As shown in Fig. 5c, these values were 3.4 and 3.5

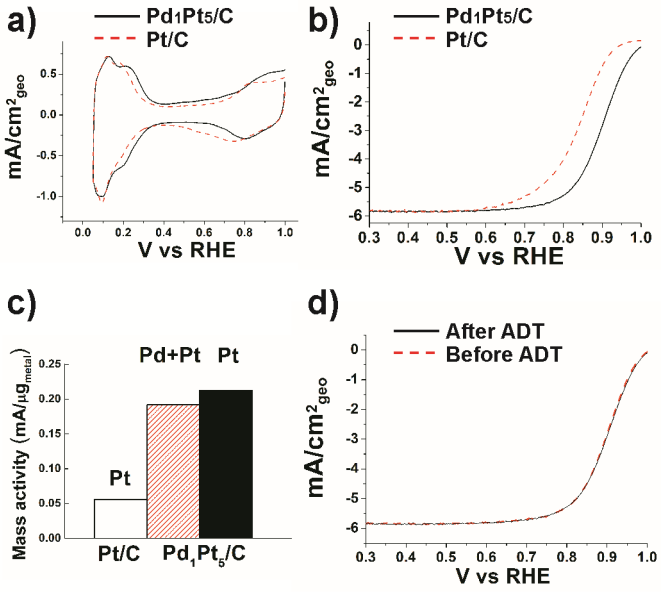

Fig. 5. Comparison of electrocatalytic activities of Pd_1Pt_5/C and commercial Pt/C. (a) Cyclic voltammograms, recorded in Ar-purged 0.1 M $HClO_4$ at RT with a sweep rate of 50 mV/s. (b) Forward-scan ORR polarization curves, recorded in O_2-purged 0.1 M $HClO_4$ at RT with a sweep rate of 20 mV/s and rotation rate of 1600 rpm. (c) Mass activities of Pd_1Pt_5/C and Pt/C measured at 0.9 V. (d) ORR polarization curves of Pd_1Pt_5/C before and after the durability test.

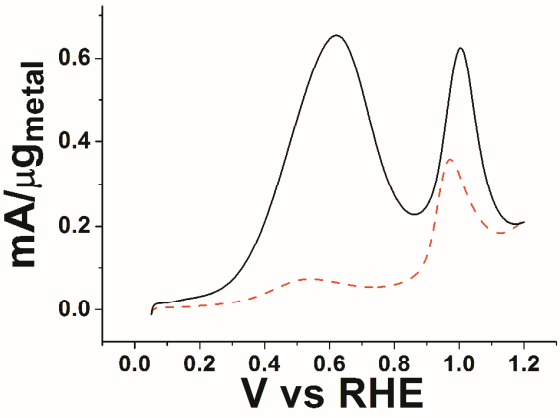

Fig. 6. Forward-scan FAOR polarization curves, recorded in Ar-purged 0.25 M formic acid in 0.1 M $HClO_4$ solution at RT, with a sweep rate of 50 mV/s. The dashed and solid lines correspond to Pt/C and Pd_1Pt_5/C.

times higher, respectively, than those of Pt/C (0.056 $mA \cdot \mu g^{-1}_{Pt}$ and 0.088 $mA \cdot cm^{-2}_{Pt}$). In addition, the Pt mass activity of Pd_1Pt_5/C (0.213 $mA \cdot \mu g^{-1}_{Pt}$) was 3.8 times higher than Pt/C. Because the activity in the oxygen reduction reaction on low-index facets increases in the order Pt {100} << Pt {111} ~ Pt {110},[52, 53] the preferential exposure of {111} would be the main reason for the enhanced ORR activity.

Fig. S13 shows the inverse current as a function of the inverse square root of the rotation rate. From the slopes of Koutecky-Levich plots, we calculated the electron transfer

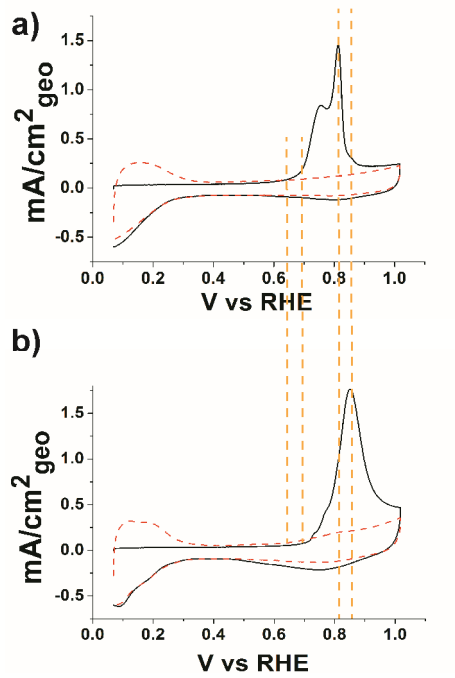

Fig. 7. CO stripping volatammograms of (a) Pd_1Pt_5/C and (b) Pt/C, recorded in in 0.1 M $HClO_4$ solution at RT, with a sweep rate of 50 mV/s. The dashed and solid curves correspond to voltammograms before and after CO exposure, respectively.

numbers at various potentials, using the published values of the kinematic viscosity of the solution (1.009×10^{-2} cm^2 s^{-1}),[54] diffusion coefficient of O_2 (1.93×10^5 cm^2 s^{-1}),[54] and the concentration of dissolved O_2 (1.26×10^{-3} mol L^{-1})[55] in $HClO_4$ solution (Fig. S13b). At 0.6 V, the constant B value was calculated to be 0.0916 mA $s^{-1/2}$, which was very similar to the expected B value of 0.0915 mA $s^{-1/2}$ for a four-electron reduction of oxygen.

The accelerated durability test (ADT) was performed by cycling the potential between 0.5 and 1.1 V for 2,000 cycles. The half wave potential of Pt/C was negatively shifted by ~30 mV after the durability test (Fig. S14). In comparison with Pt/C, the ORR curve of the Pd_1Pt_5/C was almost unchanged after the durability test (Fig. 5d). The enhanced durability might be attributed to the core-shell like structure of the Pd_1Pt_5/C with Pt-enriched surface.[56] Fig. 5 and S15 show the polarization curves of the FAOR on the Pd_1Pt_5 dendrites/C and Pt/C. It is well known that formic acid is oxidized on Pt by a dual-path mechanism.[52, 57-60] When the FAOR is governed by a direct mechanism, formic acid is dehydrogenated to produce CO_2. The dehydration path involves the formation of CO_{ad} on Pt, which acts either as a poisoning species or a reactive intermediate depending on the potential.[57, 59] The polarization curve for the Pd_1Pt_5 dendrites shows a much higher mass activity (0.452 mA·μg^{-1}_{metal} at 0.5 V and 0.622 mA·μg^{-1}_{metal} at 1.0 V) than Pt/C (0.073 mA·μg^{-1}_{Pt} at 0.5 V and 0.321 mA·μg^{-1}_{Pt} at 1.0 V). It is noteworthy to point out that the enhancement factor is much higher at 0.5 V than that at 1.0 V, suggesting the improved CO tolerance of Pd_1Pt_5 dendrites.[59, 61] According to previous studies on Pd-Pt alloys and Pd-modified Pt surfaces, Pd and Pt show a synergistic effect to enhance the activity of the FAOR by reducing or removing the strength of the CO_{ad} adsorption.[57, 59, 62, 63]

To further investigate the CO tolerance of the Pd_1Pt_5 NCs, CO stripping was carried out. Interestingly, the peak splitting was observed on the CO stripping profile of Pd_1Pt_5/C (Fig. 7a). Since the CO oxidation is the structure sensitive reaction, modifications in the number and nature of surface sites cause the change in CO oxidation profiles, often leading to the peak splitting.[64, 65] It might be interpreted that the peak at most negative potential (~ 0.75 V) is a result of the oxidation of CO on the terraces, while the peak at most positive potential (~ 0.81 V) is a result of the oxidation of CO on the edge and corner sites.[65] The peak splitting might be attributed to the increased fraction of terrace sites of Pd_1Pt_5 NCs with anisotropic rather than spherical branches. The onset potential for Pd_1Pt_5/C was negatively shifted by 50 mV with respect to that for Pt/C (Fig. 7, inset; dashed lines). The potential at maximum current of CO oxidation for the Pd_1Pt_5/C is also negatively shifted by 50 mV than that for the Pt/C, supporting the improved CO tolerance of Pd_1Pt_5/C. Added to the enhanced CO tolerance, dendritic structures have been shown to exhibit enhanced catalytic activity for the FAOR, owing to their unique porous morphology with rough surfaces.[30, 36, 39] The enhanced activity for the oxidation of formic acid on the Pd_1Pt_5 dendrites could therefore be attributed to the synergistic effect of Pd and Pt combined with its dendritic morphology.

Conclusions

In summary, we have developed a direct one-step synthetic route to Pd-Pt structures with controllable shape, size, and composition using KBr as a structure-directing agent. Using this method, various nanostructures with different compositions were successfully synthesized. As a model system, the Pd_1Pt_5 branched structures were tested as electrocatalysts and were seen to exhibit enhanced activity for the ORR and FAOR. Because this method provides rapid synthetic routes to Pd-Pt NCs with various shape, size, and composition, it may be helpful in screening active catalysts in various kinds of catalysis.

Acknowledgements

This research was supported by the MSIP(Ministry of Science, ICT and Future Planning), Korea, under the "IT Consilience Creative Program" (NIPA-2014-H0201-14-1001). This work was further supported by the National Research Foundation of Korea (NRF) grant funded by the Korea government (MEST) (No. 2012R1A2A2A01002879). This work was also supported by a grant of the Korea Health 21 R&D Project of Ministry of Health & Welfare (HI12C1515).

Notes and references

[a] Department of Chemical Engineering, Pohang University of Science and Technology (POSTECH), Pohang, 790-784 (Korea)

[b] Department of Applied Chemistry, Kyoungpook National University, Daegu, 702-701 (Korea)
*. Corresponding author: (+82) 054-279-5528,
E-mail: jinwoo03@postech.ac.kr

Electronic Supplementary Information (ESI) available: Fig. S1-S15 and Table S1-2. See DOI: 10.1039/b000000x/

1. J. Chen, B. Lim, E. P. Lee and Y. Xia, *Nano Today*, 2009, **4**, 81-95.
2. Z. Peng and H. Yang, *Nano Today*, 2009, **4**, 143-164.
3. Y. Li and G. A. Somorjai, *Nano Lett.*, 2010, **10**, 2289-2295.
4. M. Jin, H. Liu, H. Zhang, Z. Xie, J. Liu and Y. Xia, *Nano Res.*, 2010, **4**, 83-91.
5.. R. Narayanan and M. A. El-Sayed, *Nano Lett.,* 2004, **4**, 1343-1348.
6. R. Narayanan and M. A. El-Sayed, *J. Am. Chem. Soc.*, 2004, **126**, 7194-7195.
7. N. Tian, Z.-Y. Zhou, S.-G. Sun, Y. Ding and Z. L. Wang, *Science*, 2007, **316**, 732-735.
8. A. R. Tao, S. Habas and P. Yang, *Small*, 2008, **4**, 310-325.
9. B. Lim and Y. Xia, *Angew. Chem. Int. Ed.*, 2011, **50**, 76-85.
10. J. Park, J. Joo, S. G. Kwon, Y. Jang and T. Hyeon, *Angew. Chem. Int. Ed.*, 2007, **46**, 4630-4660.
11. J. Park, E. Lee, N.-M. Hwang, M. Kang, S. C. Kim, Y. Hwang, J.-G. Park, H.-J. Noh, J.-Y. Kim, J.-H. Park and T. Hyeon, *Angew. Chem. Int. Ed.*, 2005, **44**, 2872-2877.
12. B. Y. Xia, W. T. Ng, H. B. Wu, X. Wang and X. W. Lou, *Angew. Chem. Int. Ed.*, 2012, **51**, 7213-7216.
13. C. Koenigsmann, W.-p. Zhou, R. R. Adzic, E. Sutter and S. S. Wong, *Nano Lett.*, 2010, **10**, 2806-2811.
14. S. Sun, G. Zhang, D. Geng, Y. Chen, R. Li, M. Cai and X. Sun, *Angew. Chem. Int. Ed.*, 2011, **50**, 422-426.
15. B. Y. Xia, H. B. Wu, Y. Yan, X. W. Lou and X. Wang, *J. Am. Chem. Soc.*, 2013, **135**, 9480-9485.
16. T. S. Ahmadi, Z. L. Wang, A. Henglein and M. A. El-Sayed, *Chem. Mater.*, 1996, **8**, 1161-1163.
17. H. Lee, S. E. Habas, S. Kweskin, D. Butcher, G. A. Somorjai and P. Yang, *Angew. Chem. Int. Ed.*, 2006, **45**, 7824-7828.
18. C. Wang, H. Daimon, T. Onodera, T. Koda and S. Sun, *Angew. Chem. Int. Ed.*, 2008, **47**, 3588-3591.
19. C.-K. Tsung, J. N. Kuhn, W. Huang, C. Aliaga, L.-I. Hung, G. A. Somorjai and P. Yang, *J. Am. Chem. Soc.*, 2009, **131**, 5816-5822.
20. H. Song, F. Kim, S. Connor, G. A. Somorjai and P. Yang, *J. Phys. Chem. B*, 2004, **109**, 188-193.
21. A. Rodriguez, C. Amiens, B. Chaudret, M.-J. Casanove, P. Lecante and J. S. Bradley, *Chem. Mater.*, 1996, **8**, 1978-1986.
22. C.-Y. Chiu, Y. Li, L. Ruan, X. Ye, C. B. Murray and Y. Huang, *Nat. Chem.*, 2011, **3**, 393-399.
23. Y. Kang, J. B. Pyo, X. Ye, R. E. Diaz, T. R. Gordon, E. A. Stach and C. B. Murray, *ACS Nano*, 2012, **7**, 645-653.
24. J. Yang, J. Yang and J. Y. Ying, *ACS Nano*, 2012, **6**, 9373-9382.
25. Y. Song, Y. Yang, C. J. Medforth, E. Pereira, A. K. Singh, H. Xu, Y. Jiang, C. J. Brinker, F. van Swol and J. A. Shelnutt, *J. Am. Chem. Soc.*, 2003, **126**, 635-645.
26. L. Ma, C. Wang, M. Gong, L. Liao, R. Long, J. Wang, D. Wu, W. Zhong, M. J. Kim, Y. Chen, Y. Xie and Y. Xiong, *ACS Nano*, 2012, **6**, 9797-9806.
27. L. Wang and Y. Yamauchi, *J. Am. Chem. Soc.*, 2009, **131**, 9152-9153.
28. L. Wang and Y. Yamauchi, *Chem. Mater.*, 2009, **21**, 3562-3569.
29. D. Wang, Y. Yu, H. L. Xin, R. Hovden, P. Ercius, J. A. Mundy, H. Chen, J. H. Richard, D. A. Muller and F. J. DiSalvo, *Nano Lett.*, 2012, **12**, 5230-5238.
30. L. Wang, H. Wang, Y. Nemoto and Y. Yamauchi, *Chem. Mater.*, 2010, **22**, 2835-2841.
31. Y. Ye, J. Joo, B. Lim and J. Lee, *Chem. Eur. J*, 2012, **18**, 2797-2801.
32. X. Teng and H. Yang, *Nano Lett.*, 2005, **5**, 885-891.
33. M. Prochaska, J. Jin, D. Rochefort, L. Zhuang, F. J. DiSalvo, H. D. Abruña and R. B. van Dover, *Rev. Sci. Instrum.*, 2006, **77**, 054104.
34. E. Casado-Rivera, D. J. Volpe, L. Alden, C. Lind, C. Downie, T. Vázquez-Alvarez, A. C. D. Angelo, F. J. DiSalvo and H. D. Abruña, *J. Am. Chem. Soc.*, 2004, **126**, 4043-4049.
35. B. Lim, M. Jiang, P. H. Camargo, E. C. Cho, J. Tao, X. Lu, Y. Zhu and Y. Xia, *Science*, 2009, **324**, 1302-1305.
36. B. Lim, M. Jiang, T. Yu, P. H. C. Camargo and Y. Xia, *Nano Res.*, 2010, **3**, 69-80.
37. Z. Peng and H. Yang, *J. Am. Chem. Soc.*, 2009, **131**, 7542-7543.
38. L. Wang, Y. Nemoto and Y. Yamauchi, *J. Am. Chem. Soc.*, 2011, **133**, 9674-9677.
39. L. Wang and Y. Yamauchi, *Chem. Asian J.*, 2010, **5**, 2493-2498.
40. Y. Kang, X. Ye, J. Chen, Y. Cai, R. E. Diaz, R. R. Adzic, E. A. Stach and C. B. Murray, *J. Am. Chem. Soc.*, 2012, **135**, 42-45.
41. X. Huang, Y. Li, Y. Li, H. Zhou, X. Duan and Y. Huang, *Nano Lett.*, 2012, **12**, 4265-4270.
42. J. Zhang, K. Sasaki, E. Sutter and R. R. Adzic, *Science*, 2007, **315**, 220-222.43.
43. H. Ataee-Esfahani, L. Wang, Y. Nemoto and Y. Yamauchi, *Chem. Mater.*, 2010, **22**, 6310-6318.
44. L. Wang and Y. Yamauchi, *J. Am. Chem. Soc.*, 2010, **132**, 13636-13638.
45. S. Guo, J. Li, S. Dong and E. Wang, *J. Phys. Chem. C*, 2010, **114**, 15337-15342.
46. X. Huang, E. Zhu, Y. Chen, Y. Li, C.-Y. Chiu, Y. Xu, Z. Lin, X. Duan and Y. Huang, *Adv. Mater.*, 2013, **25**, 2974-2979.
47. W. Wang, D. Wang, X. Liu, Q. Peng and Y. Li, *Chem. Commun.*, 2013, **49**, 2903-2905.
48. J. Monzó, M. T. M. Koper and P. Rodriguez, *ChemPhysChem*, 2012, **13**, 709-715.
49. L. Wang and Y. Yamauchi, *Chem. Asian J.*, 2010, **5**, 2493-2498.
50. M. Jin, H. Liu, H. Zhang, Z. Xie, J. Liu and Y. Xia, *Nano Res.*, 2010, **4**, 83-91.
51. A. Mohanty, N. Garg and R. Jin, *Angew. Chem. Int. Ed*., 2010, **49**, 4962-4966.
52. N. M. Marković and P. N. Ross Jr, *Surf. Sci. Rep.*, 2002, **45**, 117-229.
53. V. R. Stamenkovic, B. Fowler, B. S. Mun, G. Wang, P. N. Ross, C. A. Lucas and N. M. Marković, *Science*, 2007, **315**, 493-497.
54. N. M. Marković, H. A. Gasteiger, B. N. Grgur and P. N. Ross, *J. Electroanal. Chem.*, 1999, **467**, 157-163.
55. M. H. Shao, T. Huang, P. Liu, J. Zhang, K. Sasaki, M. B. Vukmirovic and R. R. Adzic, *Langmuir*, 2006, **22**, 10409-10415.
56. Y. Lim, S. K. Kim, S.-C. Lee, J. Choi, K. S. Nahm, S. J. Yoo and P. Kim, *Nanoscale*, 2014, **6**, 4038-4042.

57. M. Arenz, V. Stamenkovic, T. J. Schmidt, K. Wandelt, P. N. Ross and N. M. Markovic, *Phys. Chem. Chem. Phys.*, 2003, **5**, 4242-4251.
58. A. Capon and R. Parsons, *J. Electroanal. Chem.*, 1973, **45**, 205-231.
59. J. D. Lović, A. V. Tripković, S. L. Gojković, K. D. Popović, D. V. Tripković, P. Olszewski and A. Kowal, *J. Electroanal. Chem.*, 2005, **581**, 294-302.
60. A. Więckowski and J. Sobkowski, *J. Electroanal. Chem.*, 1975, **63**, 365-377.
61. S. Yang and H. Lee, *ACS Catal.*, 2013, **3**, 437-443.
62. P. K. Babu, H. S. Kim, J. H. Chung, E. Oldfield and A. Wieckowski, *J. Phys. Chem. B*, 2004, **108**, 20228-20232.
63. H. Lee, S. E. Habas, G. A. Somorjai and P. Yang, *J. Am. Chem. Soc.*, 2008, **130**, 5406-5407.
64. J. Solla-Gullón, F. J. Vidal-Iglesias, E. Herrero, J. M. Feliu and A. Aldaz, *Electrochem. Commun.*, 2006, **8**, 189-194.
65. S. Guerin, B. E. Hayden, C. E. Lee, C. Mormiche, J. R. Owen, A. E. Russell, B. Theobald and D. Thompsett, *J. Comb. Chem.*, 2003, **6**, 149-158.

TOC

A direct one-step synthetic route to Pd-Pt nanostructures with controllable shape, size, and composition was developed for electrocatalytic applications